Highlights

Uncovering the Hidden Structure: A Study on the Feasibility of Induction Thermography for Fiber Orientation Analysis in CFRP Composites using 2D-FFT

Renil Thomas Kidangan,Sreedhar Unnikrishnakurup,C V Krishnamurthy,Krishnan Balasubramaniam

- Proposed approach accurately identifies fiber orientations and stacking sequence in CFRP laminates up to 12 layers.
- Circular induction coil produces distinct heating patterns containing pertinent information on fiber orientations
- Two-dimensional Fast Fourier transform-based image processing tool extracts spatial features to identify fiber orientations.

Uncovering the Hidden Structure: A Study on the Feasibility of Induction Thermography for Fiber Orientation Analysis in CFRP Composites using 2D-FFT

Renil Thomas Kidangan[a,*], Sreedhar Unnikrishnakurup[b,*], C V Krishnamurthy[c] and Krishnan Balasubramaniam[a]

[a] *Center for Nondestructive Evaluation (CNDE), Indian Institute of Technology Madras, Chennai 600036, India*

[b] *Institute of Materials Research and Engineering (IMRE), Agency for Science, Technology and Research (A*STAR), 2 Fusionopolis Way, Innovis #08-03, Singapore 138634, Republic of Singapore*

[c] *Department of Physics, Indian Institute of Technology Madras, Chennai 600036, India*

ARTICLE INFO

Keywords:
CFRP
Induction Thermography
NDT
Fiber orientations
2D-FFT
Inverse 2D-FFT
Quality Control

ABSTRACT

The induction heating process elicits a heating response in a carbon fiber reinforced polymer (CFRP) composite distinctly different from those in metal. Prior work in our lab and elsewhere has established that the intensity and spatial distribution of the heating patterns are governed by the fiber orientations in each layer and the degree of electrical contact between layers. Based on more extensive work on this non-conventional heating behavior, we show that the analysis of induction heating patterns enables the characterization of the fiber orientations and stacking order within the material. In the first step, 2D Fast Fourier Transform (2D-FFT) is used to extract the fiber orientations from the spatial characteristics of the heating pattern recorded with an infrared camera. In the next step, the extracted fiber orientation is used to design bandpass filters to carry out the inverse 2D-FFT and obtain the layer stacking order. Our findings demonstrate that this approach can accurately identify the layer orientations (maximum error of 6^o) and the stacking sequence in quasi-isotropic CFRP laminates with up to 12 layers. We believe that the proposed approach has the potential as a valuable nondestructive, non-contact tool for large-area inspection and quality control in manufacturing fiber-reinforced composites.

1. Introduction

Carbon Fiber Reinforced Plastics (CFRP) are composite materials composed of carbon fibers embedded in a polymer matrix. Such materials are becoming increasingly popular for lightweight yet sturdy components, such as those used in aero planes or automobiles, because of their high strength-to-weight ratios [1]. This means that they can be designed to be both strong and lightweight, which is especially desirable in aerospace engineering applications [2].

The use of CFRP provides a wide range of design options for material properties, enabling structural components to be customized to specific loads while reducing overall weight. However, this also leads to non-uniformity in composite materials, in which the strength and stiffness are determined by the placement and orientation of individual fiber strands. To achieve the desired properties of a component, it is crucial to correctly orient the fiber material. Neglecting to do so increases the risk of assembly errors and structural failure, as even a slight misalignment of just 10° can result in a 30% or more decrease in compression strength for unidirectional composites [3, 4], and changes in its response to

No external funding was received for conducting this study.

*Corresponding author

ktrenil@gmail.com (R.T. Kidangan); sreedharun@imre.a-star.edu.sg (S. Unnikrishnakurup)

impacts [5, 6]. Misalignment and stacking errors can occur during the layup process of complex geometries, which can affect the mechanical and thermal properties of the laminate structure [7, 8]. Ensuring proper layup of the fiber material is essential to avoiding potential failure and achieving the desired material characteristics.

Different techniques have been developed for this purpose, including both non-destructive and destructive methods. In the laboratory, the fiber orientation of composite laminates is typically determined destructively by obtaining a small sample from the waste edge and analyzing it using an optical microscope [9]. Non-destructive techniques such as X-ray radiography [10–13], optical sensing [14, 15], polarization imaging [16], digital image correlation [17], eddy current testing [18–20], and ultrasonic-wave scanning [21–23] has been widely tested for the measurement of fiber orientation in composite materials. Each of these techniques offers specific advantages and disadvantages, and the choice of method depends on the particular application and the desired level of accuracy. However, determining the depth-resolved fiber layup in a non-destructive manner is a challenging task. This is because it requires the identification of the orientation of individual layers at different depths within the panel. However, the non-contact inductive sensing-based eddy-current testing (ECT) [18–20] and ultrasonic pulse-echo [23] methods have shown some success in depth-resolved orientation prediction in CFRP. Both ECT and ultrasonic pulse-echo methods obtain measurements for a limited area of a sample, with ECT measuring electrical properties locally on the surface while ultrasonic pulse-echo employs a point measurement. As a result, scanning systems are required for these techniques to test large areas.

Active Infrared Thermography (IRT) is a rapidly growing Non-Destructive Testing (NDT) method that offers several benefits, including quick, non-contact inspections of materials and full-field evaluations [24]. Active thermography involves the introduction of heat into material using an external source, such as an optical source (optical thermography) [25], vibration (vibrothermography) [26], or induction heating (induction thermography) [27, 28], to create a transient condition for the detection of defects or the analysis of material properties by monitoring the temperature decay on the surface. This approach has gained popularity due to its non-destructive and non-contact nature, making it an attractive method for the inspection and characterization of various materials, including composites [29], metals [30], and ceramics [31]. There have been a few studies to detect fiber orientation in composites using active IRT [32–34]. Fernandes et al. introduced a novel approach utilizing a diode-laser beam for localized heating of a small spot on the surface of a CFRP laminate [32, 34]. The heat pattern was then observed using an infrared camera, and a method was proposed to extract the local fiber orientation from the resulting infrared sequence. In their study, Wang et al. employed a depth dynamic-resolution thermal-wave radar imaging technique to detect fiber lay-up orientations in a unidirectional CFRP laminate composite [33]. They proposed a phase characteristic of the thermal wave radar signal, calculated using a discrete fractional Fourier transform, and demonstrated its usefulness in identifying the fiber layup orientation at different depths within the composite. These studies were either limited to the inspection of the layer orientation on the surface layer or used a numerical model and inverse analysis with the aid of high computational

power.

This paper uses active infrared thermography to analyze the internal structure of unidirectional fabric-based (prepreg, non-crimp) composite materials. Our method uses induction heating to thermally stimulate the CFRP laminates. The presence of electrically conductive carbon fibers makes induction heating possible in CFRP laminates. However, the heating response of CFRP laminates is different from metals. The CFRP laminates produce distinctive heating patterns governed by the fiber orientation and the degree of electrical contact between various layers. This non-conventional heating behavior has been extensively investigated in this paper to identify the fiber orientations and characterize the stacking order within the material. An infrared camera is used to record the sample's heating and cooling profiles. The obtained thermal image sequence contains geometrical patterns owing to the fiber directions, which were then processed using a two-dimensional Fast Fourier transform (2D-FFT). The amplitude spectrum obtained from the transformation is used as the primary tool for identifying the fiber orientation within the composite, with a maximum error in identifying the fiber orientation with respect to the designed orientation of 6^o. Our method provides a non-destructive and efficient way to assess the layer orientation of unidirectional fabric-based composite materials, making it a valuable tool in the field of material science and engineering. The extracted fiber orientations are used to design bandpass filters for carrying out the inverse 2D-FFT to obtain the layer stacking order. The stacking sequence was correctly predicted for up to 12 layers in quasi-isotropic CFRP laminates.

This study is structured as follows: In the subsequent section (Section 2.1, we will present the materials and methods, including an overview of induction heating mechanisms in CFRP composites, how the understanding of heating mechanisms lead to the proposed approach, the preparation of samples, and the novel method proposed for extracting fiber orientation and the stacking sequence. In Section 3, we will present the results obtained from the study. Finally, we will present our summary and conclusions in Section 4.

2. Materials and Methods

2.1. Induction Heating mechanism in CFRP composites

The induction heating mechanism in CFRP composites offers a unique heating response due to the presence of discrete electrically conductive carbon fibers. The direction of the carbon fibers in the laminate determines the specific pattern in which the induced current is permitted to flow. Hence, two scenarios can arise in a unidirectional carbon fiber layer (single layer of fabric or multiple layers of fabric aligned in the same direction). Scenario-1, where induced current completes the loop within the fiber itself, and scenario-2, where induced current completes the loop by passing through the carbon fibers along the axial and transverse directions. The flow of induced current in the transverse direction is only possible through the random contacts of fiber along the axial direction or/and the capacitive coupling

between the fiber and the polymer medium. Wasselynck et al. [35] studied both scenarios solving electromagnetic and electrostatic equations and calculated the impedance values for the scenarios. They found the impedance for completing the current loops within the fiber to be very high compared to the impedance due to the capacitive coupling between the fibers (the ratio is in the order of 10^{13}). Hence, they concluded that the possibility of current loops ending within the fiber to be negligible. Though the impedance due to the capacitive coupling between the fibers is less than the impedance for completing the current loop within a fiber, this is not a sufficient condition for observing heating in the unidirectional laminate. It is widely reported [36, 37] that unidirectional laminates cannot be heated using the induction principle due to the absence of closed current paths. This observation disagrees with the fact that fibers have random contacts throughout the laminate for fiber volume fractions greater than 30%. Prakash et al. [38] have reported that at low frequencies, the induced current completes the loop through the random contacts of fibers in the laminate. If the frequency is sufficiently large (> 15 MHz), the reactance of inter-fiber capacitance would be low compared to the resistance of the conduction path through contact points. Nevertheless, the heating cannot be observed in unidirectional laminates at the frequencies considered in this study. Thus, it can be concluded that in a unidirectional laminate, heating cannot be observed, even when the fibers are in contact at random points throughout their axes.

Thus, to observe heating due to induction in a unidirectional fabric-based (prepreg, non-crimp fabric) laminate, a minimum of two layers aligned in different directions is required. In a two-layer unidirectional fabric-based laminate with fibers aligned in perpendicular directions (Figure 1), the closed current paths consist of fibers along their axial directions and the interfaces between the two layers. The interfaces allow the current to flow from one layer to another through the actual contacts of fibers at the junctions and the capacitive coupling existing at the junctions if a polymer medium is present between the fibers.

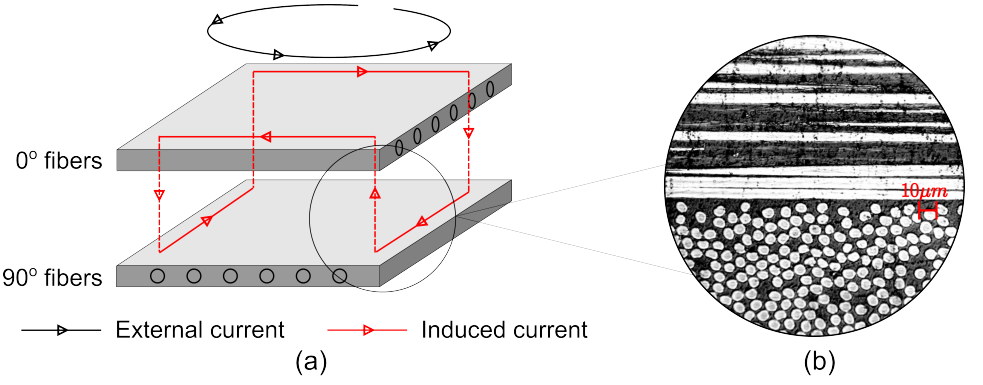

Figure 1: (a) Schematic of a two-layer unidirectional fabric-based laminate with fibers aligned in perpendicular directions and the paths of induced current (in red color) when a circular coil is used for excitation (b) The microstructure of a two-layer laminate

When CFRP laminates are exposed to an alternating magnetic field, heating can occur due to (a) Joule loss in fiber [37, 39–41] (b) polymer dielectric loss exists between the fibers of adjacent plies [36, 42–44] and (c) contact

resistance at the overlapping fiber junctions due to the fiber-fiber contact [45–48]. In studies by Fink et al. [36], the dominant heating mechanism occurs in the polymer regions between the overlapping fibers. This might be true only for the cases where the fiber volume fraction is very low (< 30% according to [38]). However, Yarlagadda et al. [46] discount the dielectric hysteresis heating at the junctions by conducting two sets of experiments, the first with a pancake coil to induce alternating currents (ac) in the unidirectional prepreg loops and the second with one side of the loop cut and connected to a direct current (dc) source. Both these experiments showed similar heating rates and rise times, and since dc is not sensitive to capacitive coupling, the dielectric hysteresis heating mechanism can be ruled out. Therefore, heating along the fibers and heating at the junctions due to electrical contacts at the interfaces are the two possible heating mechanisms expected in unidirectional-based CFRP laminates. Out of two heating mechanisms, the dominant one will be determined based on fiber volume fraction, layer thickness [49], fabric type (non-crimp or prepreg), and consolidation processes [50].

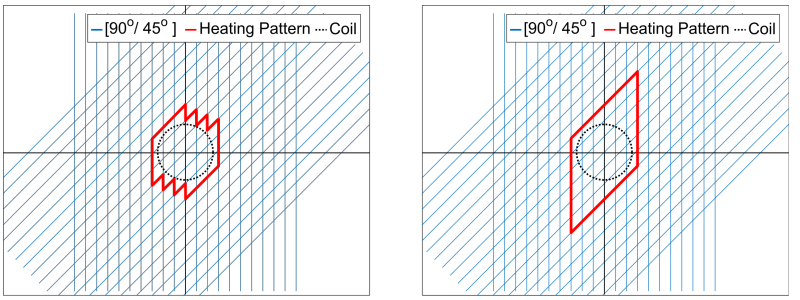

Figure 2: Schematic of two layers of carbon fibers oriented in [90/45] along with induced current paths for (a) low junction resistance case and (b) high junction resistance case.

The dominant heating mechanism and the direction of carbon fibers determine the spatial characteristics of surface temperature distribution. In two layers of carbon fibers aligned in 90^o and 45^o excited using a circular coil (Figure 2), a very low junction resistance will allow induced currents to encounter more junctions and complete the loop using the least resistive path (Figure 2a). On the other hand, if the junction resistance is high, the induced current is forced to choose the minimum possible junctions to complete the loop (Figure 2b). The former results in an approximate circular temperature pattern close to the coil diameter. The latter results in a non-circular temperature pattern bigger than the coil diameter (by almost three times). The fabrication process of the laminates and the fabric type used for fabrication result in either of the above scenarios. We have previously studied the influence of interlaminar microstructure on the induction heating patterns of CFRP and found that when a circular coil was used for the induction process on a mutually perpendicular fiber layup, the heating patterns shifted from a circular profile (low junction resistance case) to a rectangular profile (high junction resistance case) as the gap between the fibers at the interface grew [50]. The variation in the interlaminar gap results from different consolidation processes and fabric types used for the study. The

current study investigates the proposed approach on laminates that exhibited a non-circular temperature pattern when heated with a circular induction coil.

2.2. CFRP laminates used for the study

. The study was conducted on four CFRP laminates with multiple layers and fiber orientations. A minimum of four layers was selected for the fabrication due to practical considerations. The samples were prepared using the compression molding process. The fiber architecture used for the fabrication is prepreg. The compression molding process employed a pressure of 400 kg/cm^2. This pressure was applied for 2 hours at 120 ^oC and de-molded at 80 ^oC. The size of each plate is 300 mm x 300 mm, and an approximate individual layer thickness of 0.128 mm. The layup sequences of the samples were chosen to achieve a minimum of two adjacent layers oriented in different directions. This was a necessary condition to observe heating due to induction in CFRP laminates, as discussed in section 2.1. In the current study, these adjacent fiber layers are termed active pairs (AP). In a laminate, multiple active pairs, multiple inactive pairs (i.e., two adjacent layers oriented in the same direction), and repetition of existing active pairs can exist. The study was conducted on samples containing multiple active pairs such as 1, 2, 3, and 5 (table 1). In

Table 1
Details of the CFRP laminates used for the study

Sl. No.	No. of Layers	Layup Sequence	No.Active pairs	Active pairs (AP)	Sample Label
1	4	[0/90/90/0]	1	[0/90]	CFRP-4L-1P
2	4	[0/30/30/90]	2	[0/30], [30/90]	CFRP-4L-2P
3	4	[90/ ± 45/0]	3	[90/45], [±45], [−45/0]	CFRP-4L-3P
4	6	[−60/90/ ± 45/90/0]	5	[−60/90], [90/45], [±45], [−45/90], [90/0]	CFRP-6L-5P

the microstructure image of four samples considered in this study (Figure 3), each layer has been marked with the corresponding fiber orientation. Each image has been marked with vertical lines to show the active pairs involved in the induction heating process. The line colors denote the various combinations of layers available in each laminate. There are two similar active pairs and one inactive pair (2^{nd} and 3^{rd} layers in Figure 4a) in CFRP-4L-1P. The inactive pairs are so named because they cannot form a closed current path through which induced current can flow. These layers, however, are part of other active pairs in the sample (1^{st} and 2^{nd}, and 3^{rd} and 4^{th}). Similarly, two multiple active pairs and one inactive pair are found in CFRP-4L-2P (Figure 3b). In CFRP-4L-3P and CFRP-4L-5P, all the possible pairs are active.

The predicted heating patterns for each active pair available in the samples when exposed to induction heating using a circular coil (Figure 4a) were constructed based on the closed current paths each active pair can offer for the flow of induced current. The closed current paths comprise fiber orientations and the interfaces between two adjacent layers of fibers. A least resistive path for the flow of the induced current results in a non-circular heating pattern (Figure 4a).

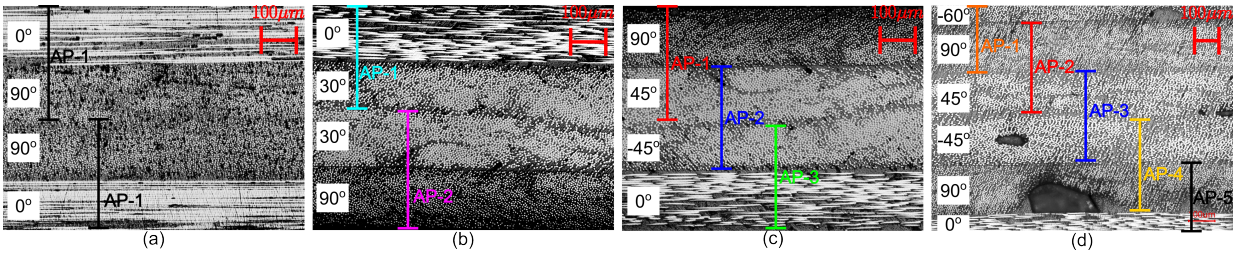

Figure 3: Microstructure images of (a) CFRP-4L-1P, (b) CFRP-4L-2P, (c) CFRP-4L-3P, and (d) CFRP-6L-5P highlighting the active pairs that take part in induction heating process and the orientation of each layer

The combined effect of all the individual heating patterns was also predicted (Figure 4b).

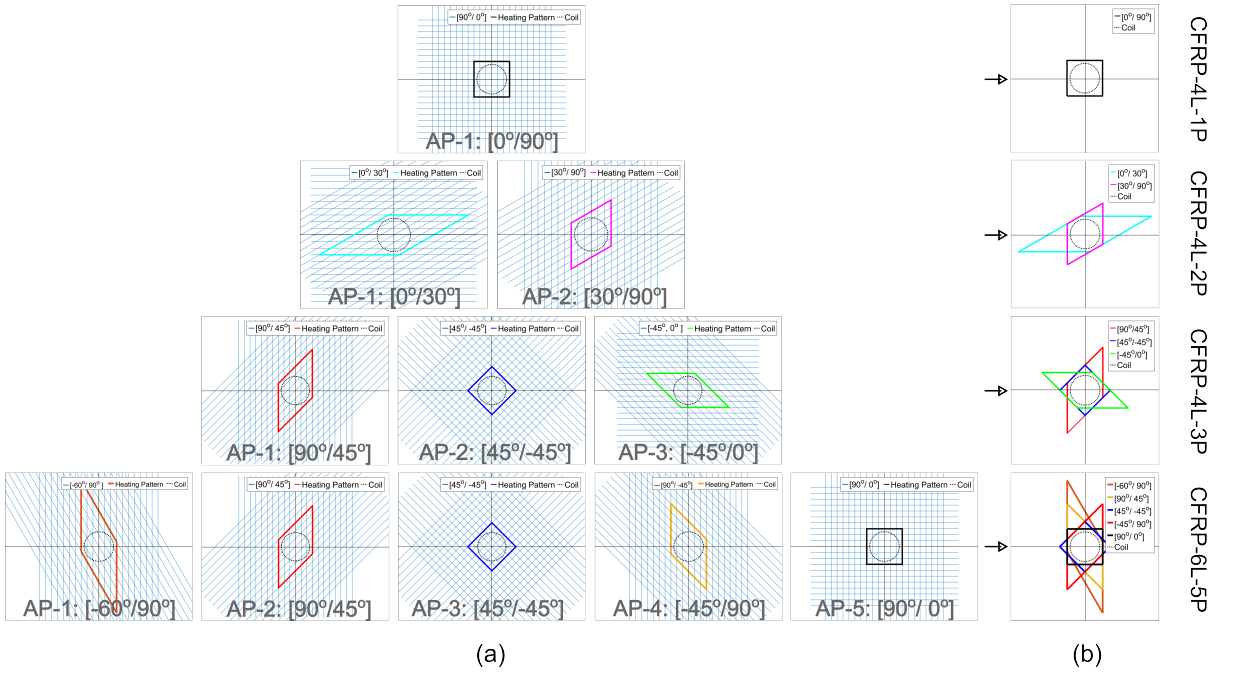

Figure 4: (a) The predicted heating patterns based on the active pairs available in the CFRP laminates considered for the study and (b) the combined heating patterns of the CFRP laminates.

2.3. Two-Dimensional Fourier Transform Analysis

The geometric characteristics of spatial domain images were extracted using two-dimensional Fourier transformation. The Fourier Transform is an important image-processing tool that is used to decompose an image into its sine and cosine components. The output of the transformation represents the image in the Fourier or frequency domain, while the input image is the spatial domain equivalent. In the Fourier domain image, each point represents a particular frequency contained in the spatial domain image. The Fourier analysis has been used extensively for textile-related applications [51–54], fiber orientation in paper sheets, biological cell networks, and also fiber reinforced polymers [18, 20]. The 2D Fourier transform was computed using the inbuilt MATLAB function FFT2 [55], which returns the

two-dimensional discrete Fourier transform (DFT) of the image. The DFT was computed with a fast Fourier transform (FFT) algorithm. Since we are concerned with digital images, the equation for performing Discrete Fourier Transformation is given below:

$$F(u,v) = \frac{1}{MN}\sum_{x=0}^{M-1}\sum_{y=0}^{N-1} f(x,y)exp\left[-j2\pi\left(\frac{ux}{M}+\frac{vy}{N}\right)\right] \tag{1}$$

where, $f(x,y)$ represents the pixel at position (x,y), whereas $F(u,v)$ is the function to represent the image in the frequency domain pertaining to the position u and v. $M \times N$ represents the dimension of the image, j is $\sqrt{-1}$ and u and v are the frequency component of the spatial wave in the x direction and y direction, respectively [56]. The solution of the 2D-FFT is complex and is computed as:

$$F(u,v) = F_R(u,v) + iF_I(u,v) \tag{2}$$

where the subscript R and I indicate the real and imaginary parts of the solution, respectively. To interpret the FFT, the amplitude at each pixel is calculated. The amplitude spectrum contains no phase information but provides the total amount of information at a given frequency. The Fourier amplitude is computed as follows:

$$|F(u,v)| = \left(F_R(u,v)^2 + F_I(u,v)^2\right)^{\frac{1}{2}} \tag{3}$$

The dynamic range of the amplitude spectrum is often mapped using logarithmic transformation as

$$F_{ln}(u,v) = ln\big(|F(u,v)|\big) \tag{4}$$

The Fourier amplitude spectrum can quantify the structural pattern in the image. To quantify the angles present in the sample, the azimuthal distribution of the radial average of the Fourier amplitude spectrum has been estimated (equation 5). This radial average can generate 1D amplitude intensity plots from which the fiber angles can be found.

$$I_{mean}(\theta) = \frac{\sum_{r=r_{min}}^{r_{max}} F_{ln}(r)}{n} \tag{5}$$

Where r_{min} and r_{max} correspond to the minimum and maximum radii considered for estimating the azimuthal distribution of the radial average of the Fourier amplitude and n corresponds to the number of pixels between two

radii. This eliminates the spectral artifacts at both low and high frequencies. The azimuthal distribution of intensity relates to the fiber orientations in the thermal image.

2.3.1. Filtering and Inverse 2D Fourier Transform

In order to filter the 2D-FFT data and recover the angle-specific thermal sequence using inverse 2D-FFT, a band-pass filter was employed. This type of filter permits frequencies within a particular range to pass through while reducing the strength of frequencies outside that range. The range of frequencies that should be allowed to pass through the filter will vary based on the frequency distribution of the pattern in both the azimuthal and radial directions. To achieve this, a 2D band-pass filter was used, which combines a low-pass filter and a high-pass filter in the radial direction. The parameters used for the radial filter, such as the angle range, radial frequency range, and bandwidth, were fixed by overlaying the filter over the amplitude image generated for a specific experiment. This filter was employed throughout the sequence of thermal images for a particular angle to analyze the moment in which a specific pattern appeared in the sequence. After the band-pass filter was applied to the 2D-FFT data, the filtered data was transformed back into the spatial domain by utilizing inverse 2D-FFT. The Inverse Discrete Fourier Transform (IDFT) is defined as:

$$f(x,y) = \frac{1}{MN}\sum_{u=0}^{M-1}\sum_{v=0}^{N-1} F(u,v) exp\left[-j2\pi\left(\frac{ux}{M}+\frac{vy}{N}\right)\right] \tag{6}$$

2.4. Experimental Setup

Experiments were carried out with a 1 kW induction heating unit attached to a single-turn circular coil with a diameter of 100 mm (Figure 5). For 500 ms, an alternating current at a frequency of 220 kHz was delivered into the coil, producing significant heat in the sample. A medium wave infrared (MWIR) camera with a frame rate of 200 Hz at full frame (320 x 256 array of pixels) was used to measure the surface temperature distribution. The samples were inspected using transmission mode. The samples are electromagnetically thin at the frequency used, which allows one to place the coil in a transmission arrangement. The distance between the coil and the sample was fixed at 3 mm. The results obtained are discussed in the next section.

3. Results and Discussion

The thermography experiment generates three-dimensional surface temperature data, with space in the first two dimensions and time in the third. All active pairs of carbon fibers available in the CFRP laminates are heated simultaneously during the induction heating. Each time frame captures the surface temperature evolution due to the heat transfer from multiple layers. This creates unique temperature patterns on the laminate surface owing to the layer orientation. A sample case is demonstrated for CFRP-4L-3P laminate (Figure 6), in which three active pairs which are

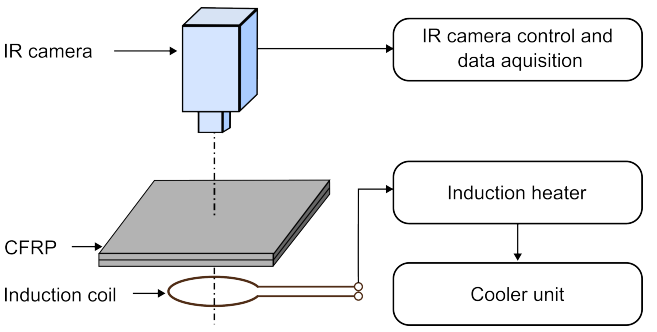

Figure 5: Schematic of experimental setup showing an infrared camera on the top, and the induction coil on the bottom of the specimen

[90/45], [45/ − 45], and [−45/0] exist. Each active pair generates heating at specific patterns. Since the current study has been conducted on the samples that show non-circular heating patterns owing to the orientation of fibers, heating patterns shown in figure 4 are expected. This behavior can be seen in the sequence of thermal images in Figure 6a to Figure 6d obtained at increasing time steps after begin of heating. The initial signs of the first active pair (AP-1: [90/45]) can be seen at $t = 0.035s$ as two vertical heating zones (Figure 6a) later joined by two inclined (45^o) heating zones at $t = 0.065s$ (Figure 6b). Similarly, a rhombus-shaped heating pattern is obtained (Figure 6c–d) which belongs to second active pair (AP-2: [45/ − 45]) at $t = 0.115s$ and $t = 0.19s$ respectively. The predicted heating patterns of the above-mentioned cases are shown in figure 6. The remaining heating patterns due to the third active pair (AP-3) cannot be distinguished from the thermal images.

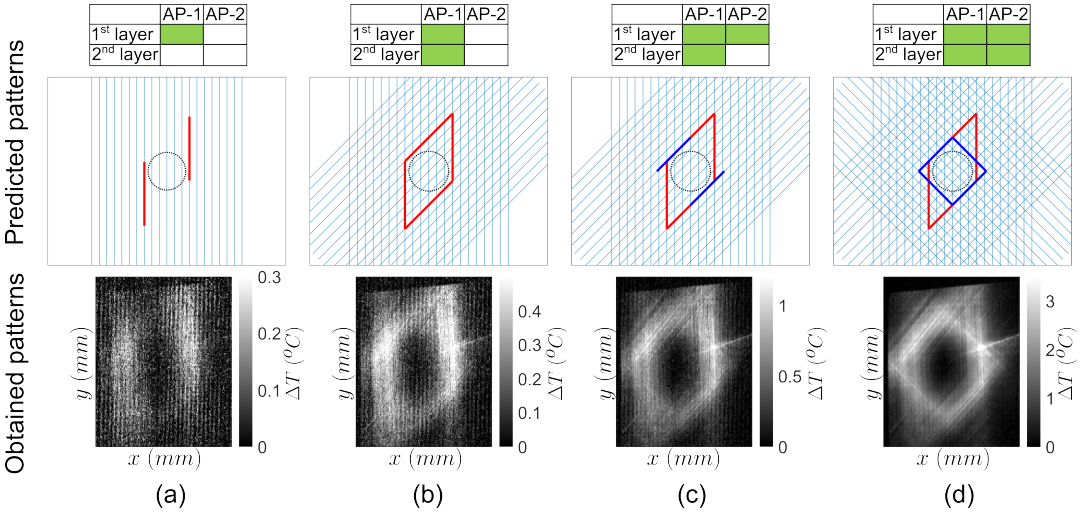

Figure 6: Evolution of surface temperature patterns for the sample: CFRP-4L-3P along with the predicted heating patterns (a) top layer of first active pair is visible at $t = 0.035s$ (b) bottom layer of first active pair is visible at $t = 0.065s$ (c) top layer of the second active pair is visible at $t = 0.115s$, and (d) bottom layer of the second active pair is visible at $t = 0.19s$.

The temperature Vs. time graph of four different locations (P1 to P4) on the CFRP-4L-3P sample is shown in figure 7. The graph contains induction heating and cooling phases. The points P1 and P2 were selected from the approximate

locations of the heating pattern caused by [90/45] active pair, and P3 and P4 were selected from the approximate locations of heating patterns caused by [45/ − 45] active pair. P1 and P3 points represent the fiber regions, while P2 and P4 points represent the junctions in active pairs. The junction heating is higher than the fiber heating for both active pairs. The topmost active pair in CFRP-4L-3P is [90/45]. Hence, the temperature response of P1 and P2 points differs from that of P3 and P4 points. The former shows a trend of decreasing temperature after induction heating, while the latter shows an opposite trend. This is attributed to the contribution of heating from the active pairs present in the sample. During the heating phase, the induced heat patterns provide valuable information about the inner structure of the specimen, including the fiber orientations. As the lateral heat diffusion is minimal during this phase, the heating patterns directly reflect the geometrical characteristics related to the fiber orientations and stacking sequence. Thus the heating phase data is used for the identification of fiber orientation and stacking sequence.

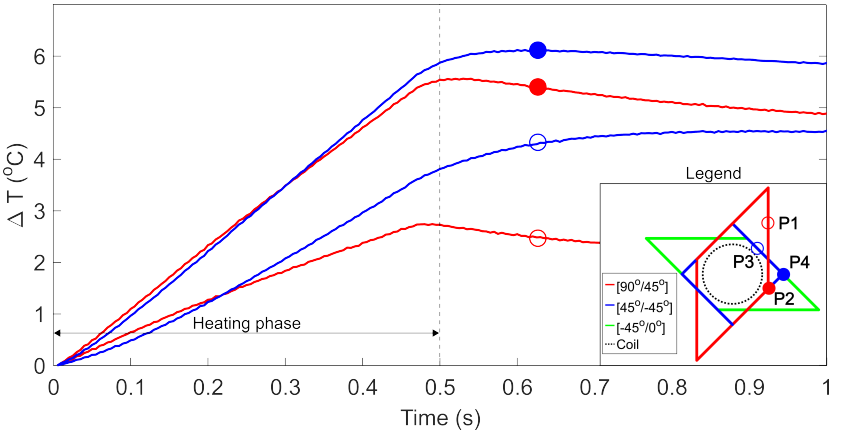

Figure 7: Sample: CFRP-4L-3P, Timing graph of four points (P1 to P4) selected on a sample thermal image. P1 and P2 points represent [90/45] active pair and P3 and P4 points represent [±45] active pair

3.1. Identification of fiber orientations

The geometrical features in the spatial domain of the thermal image is used to identify the fiber orientations in a laminate with the help of two-dimensional Fourier transformation as discussed in section 2.3. The properties of the discrete Fourier transform (DFT) of an image are the periodicity and complex conjugate symmetry. The spectrum repeats itself endlessly in both directions with periods of the width (M) and height (N) of the image. That is, $F(u,v) = F(u+kM, v+lN)$ where $k, l = [-\infty, ..., -1, 0, 1, ...\infty]$. The $M \times N$ array of Fourier coefficients $F(u,v)$ computed from $M \times N$ image with the 2D-DFT is a single period from this infinite sequence. Complex conjugate symmetry means that $|F(u,v)| = |F(-u,-v)|$, so that there exist negative frequencies which are mirror images of the corresponding positive frequencies in the amplitude spectrum. The interpretation of the spectra is made easier by centering the results of DFT such that frequency increases in any direction away from the origin. The Fourier theory treats an input image as if it were part of a periodically repeated array of identical images extending in both directions infinitely. Any discontinuity

in the periodic image results in strong vertical and horizontal components in the amplitude spectrum. This poses a serious risk in our case since the identification of fiber orientation is based on the components present in the amplitude spectrum. This risk is mitigated by windowing the image prior to DFT in such a way as to gradually reduce the pixel values to zero at the edges of the image. This ensures a smooth transition between the images when they are treated as periodically repeated arrays. A Hanning window function ($W(r)$) is defined for this purpose according to equation 7 where r is the distance of each image pixel (x, y) from the center (x_c, y_c) of the image, r_{max} is the given maximum distance.

$$W(r) = \begin{cases} 0.5 - 0.5cos[\pi(1 - \frac{r}{r_{max}})], & \text{if } r <= r_{max} \\ 0, & \text{otherwise} \end{cases} \tag{7}$$

In the identification of fiber orientations demonstrated in a CFRP-4L-1P sample (Figure 8), the input thermal image (at $t = 0.5s$) reveals a square-shaped heating pattern (Figure 8a) similar to the prediction plots (Figure 4a). In the shifted Fourier amplitude spectrum obtained from the windowed thermal image (Figure 8b), the geometrical features in the spatial domain are clearly captured in the frequency domain image. To quantify the angles present in the sample, the azimuthal distribution of the radial average of Fourier amplitude spectrum ($I_{mean}(\theta)$) has been estimated. The average amplitude of the Fourier spectrum was estimated between two radii to avoid lower and higher frequencies after performing a polar transformation (Figure 8c). The azimuthal distribution of radial average of Fourier amplitude spectrum produces a preferential weighted orientation distribution (Figure 8d). This graph corresponds to the angular distribution of intensity and can provide information about the orientation of layers in the sample based on the peak intensities. Since the direction of the corresponding frequency peak is perpendicular to the fiber direction, the real fiber angles θ_{fiber} can be determined from the frequency angles θ_{freq} according to equation 8. The result obtained after shifting is plotted in the polar graph for straightforward interpretation (Figure 8e).

$$\theta_{fiber} = \theta_{freq} - 90 \tag{8}$$

The orientations of the fibers in the CFRP-4L-1P configuration are visible in the thermal image. The frequency domain analysis yields no additional information. However, as the number of different active pairs increases, identifying fiber orientations from thermal images becomes difficult. The complexity of geometrical features present in thermal images of CFRP-4L-2P, CFRP-4L-3P, and CFRP-4L-4P is shown in the top row of figure 9.

The analysis conducted on CFRP-4L-1P is repeated for CFRP-4L-2P, CFRP-4L-3P, and CFRP-4L-5P. The fre-

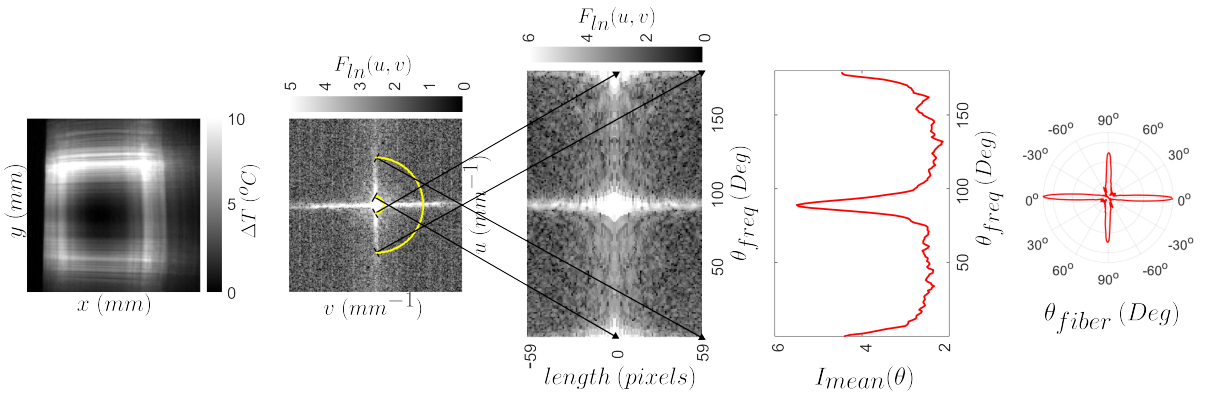

Figure 8: Sample CFRP-4L-1P (a) Thermogram at $t = 0.5s$ (b) 2D-FFT Absolute spectrum $F_{ln}(u, v)$ (c) Transformation into Polar coordinates (d) Azimuthal-distribution of radially averaged Intensity $I_{mean}(\theta)$ for frequency angles (θ_{freq}) (e) Azimuthal-distribution of $I_{mean}(\theta)$ in polar plot (θ_{fiber})

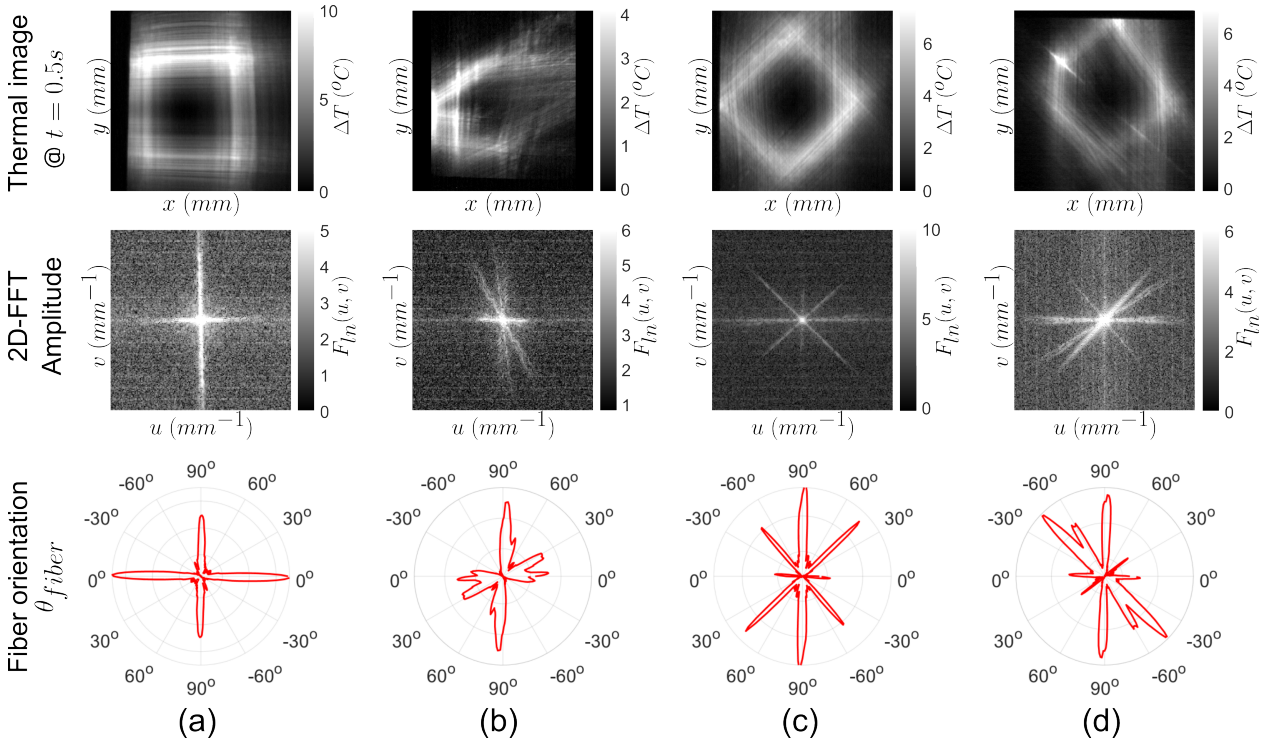

Figure 9: Thermograms at $t = 0.5s$ (top row), 2D FFT amplitude spectrum: $F_{ln}(u, v)$ (middle row) and fiber orientation: θ_{fiber} plots (bottom row) for (a) CFRP-4L-1P, (b) CFRP-4L-2P, (c) CFRP-4L-3P, and (d) CFRP-4L-5P

quency domain images and the polar plots showing the fiber orientations are shown in the second and the third rows of figure 9, with the identified fiber orientations shown in Table 2.

Table 2
Fiber orientations in the CFRP laminates identified from 2D-FFT analysis

Sample Label	Fiber orientations present in the samples	Obtained fiber orientations
CFRP-4L-1P	0, 90	1, 89
CFRP-4L-2P	0, 30, 90	6, 30, 88
CFRP-4L-3P	90, 45, −45, 0	90, 44, −48, 2
CFRP-6L-5P	−60, 90, 45, −45, 90, 0	−60, 88, 50, −47, 88, 0

3.2. Characterisation of stacking sequence

The inverse 2D-FFT method is employed to analyze the order of occurrence of each layer in the sample. Specific band pass filters across the radial Fourier amplitude for individual angles are used to recreate the orientation patterns corresponding to each layer. The process flow of the algorithm used for the layer order estimation and internal structure decomposition using inverse 2D-FFT analysis is shown in figure 10. Each step is illustrated using the sample CFRP-4L-3P.

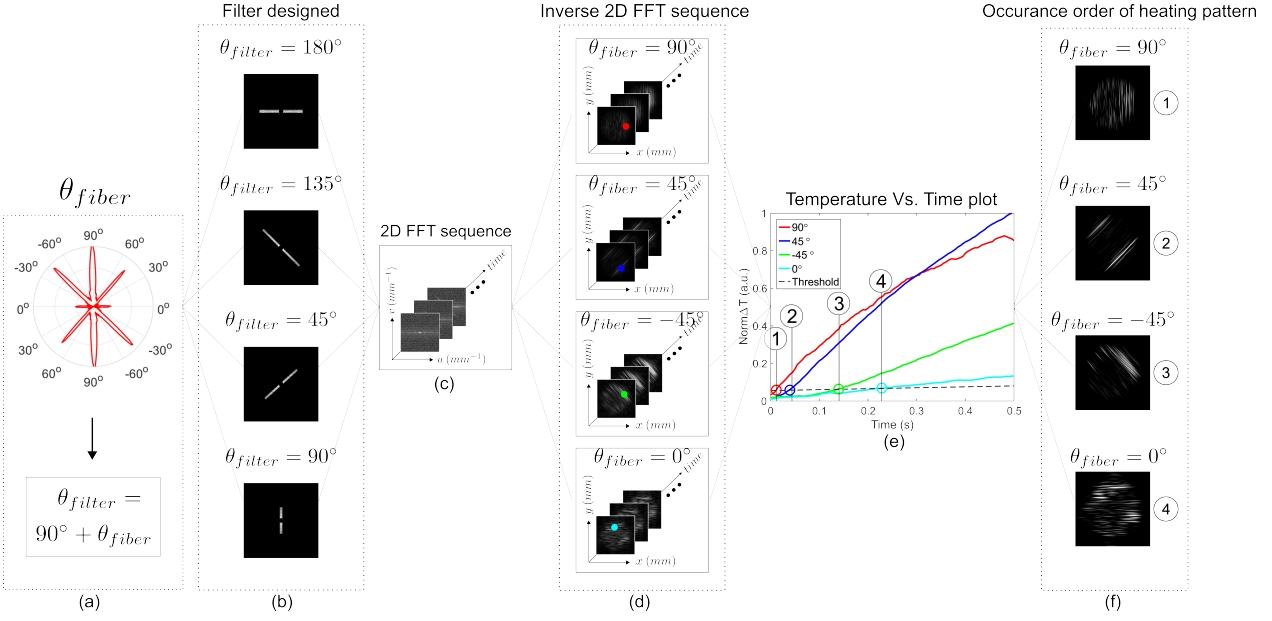

Figure 10: Process flow of the proposed algorithm for the layer order estimation and internal layer decomposition (demonstrated for sample CFRP-4L-3P). (a) Fiber orientations (θ_{fiber}) identified from 2D-FFT analysis (b) Filters designed (θ_{filter}) for each fiber orientation (c) 2D-FFT sequence (d) Inverse 2D-FFT sequence obtained for each filter (θ_{filter}) (e) Temperature-Time profiles of reference points obtained from each inverse 2D-FFT sequence highlighting the order of appearance (f) The sum of five thermal images from the threshold crossing frame from each inverse 2D-FFT sequence.

Firstly, all the dominant angles obtained from the layer orientation analysis are used for the filter design. The angles for the filter selection θ_{filter} can be determined from the fiber angles θ_{fiber} using the equation 9. In the case of sample CFRP-4L-3P, the angles are $[90/45/-45/0]$, and the designed filters undergo a low pass and high pass stop mask to

suppress the noise features (Figure 10b).

$$\theta_{filter} = 90 + \theta_{fiber} \tag{9}$$

Next, the designed bandpass filters are multiplied with the Fourier amplitude sequence for each angle. Each multiplication will generate a sequence of filtered data. In the next step, an inverse 2D-FFT operation is performed on these individual sequences to generate a new sequence that represents the thermal distribution corresponding to the individual layers (Figure 10d). During the induction heating process, all the active pairs available in the laminate are heated. As a result of heat diffusion, thermal patterns appear on the measurement surface over time, depending on the layer orientation and depth. By analyzing the time-dependent inverse 2D-FFT data, the order of occurrence for each layer can be deduced. From each of the inverse 2D-FFT sequences, the temperature-time profiles are plotted at the corresponding localized pattern region averaged over nine pixels and plotted together to identify the time shift due to the heat diffusion. For sample CFRP-4L-3P, three active heating pairs are present. It can be observed from the temperature profiles of these filtered data sequences (Figure 10e) that the temperature rise due to the 90° layer angle occurs first, and the temperature rise in subsequent layers occurs with a temporal shift. To elucidate the order of appearance, we used the temperature increase above a predetermined threshold value. The threshold value is calculated as twice the NETD (Noise Equivalent Temperature Difference) of the infrared camera utilized in the study. The heating pattern obtained suggests that the shift in temperature rise resulting from heat diffusion from the internal layers can be effectively imaged using the inverse 2D-FFT approach. The order of appearance has been numbered and highlighted in the ascending order at which each orientation appeared on the sample surface (See Figure 10e). The sum of 5 thermal images from the threshold crossing frame from each sequence is selected and represented in Figure 10f. The temperature patterns owing to the respective fiber orientations can be seen in these images.

For each sample, the filtering and inverse 2D-FFT analysis is performed on the Fourier amplitude image sequence to determine the order of pattern occurrence. Similar findings can be observed in Figure 11a, b, c, and d for samples CFRP-4L-1P, CFRP-4L-2P, CFRP-4L-3P, and CFRP-6L-5P, respectively. The time at which the threshold crossing occurs is delayed with an increase in the number of layers.

The inverse 2D-FFT analysis decomposed the individual heating patterns corresponding to the internal layers and separated the temperature rise (Figure 12a), whereas this separation is not observed in the raw thermogram ((Figure 12b). The threshold crossing locations are zoomed and highlighted as an inset in figure 12b. Hence, the raw thermogram contains insufficient information to deduce the layer stacking sequence. This highlights the capability of the proposed approach to determine the order of pattern occurrence.

An attempt has been made to identify the stacking sequence of the samples using the information obtained from

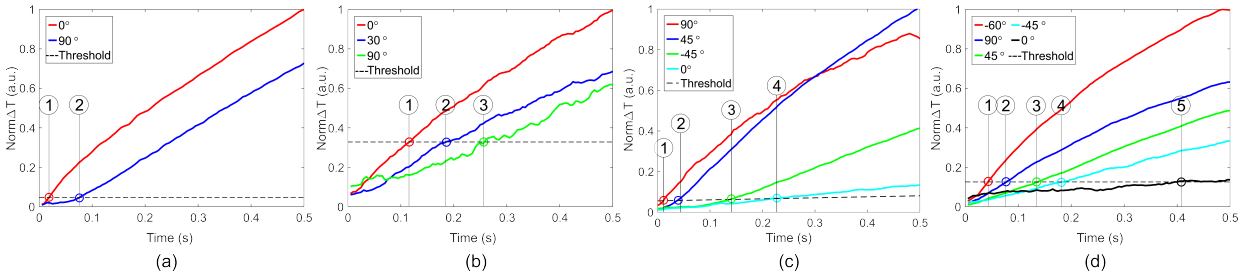

Figure 11: Normalized Temperature-time profile from filtering and inverse 2D-FFT analysis (a) CFRP-4L-1P, (b) CFRP-4L-2P, (c) CFRP-4L-3P, and (d) CFRP-6L-5P

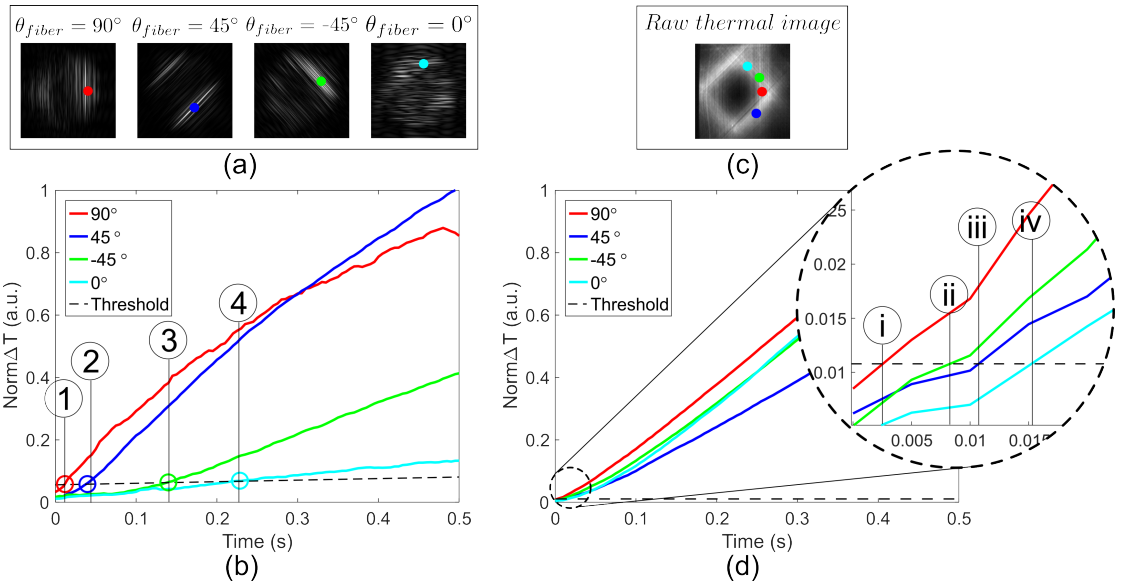

Figure 12: Temperature-time profile comparison between inverse Fourier analysis-based approach and raw thermogram for CFRP-4L-3P case

2D-FFT and inverse 2D-FFT analysis. The former gives information about the fiber orientations present in the samples, and the latter provides the order of pattern occurrence. Notably, this approach could capture information from both sides of the specimen, enhancing the results' accuracy and robustness. Furthermore, stacking sequences were identified by leveraging established guidelines for the fabrication of CFRP panels. Layer combinations that satisfy both orders of pattern occurrence impose strong constraints on the possible solutions of stacking sequence than those that satisfy only one order of pattern occurrence. The proposed approach, when interpreted along with the guidelines for CFRP fabrication, results in unique solutions for its stacking sequence. For example, in the CFRP-4L-1P case, both front and back inspections resulted in the order of occurrence of [0/90]. The knowledge of cross-play laminate architecture enables us to identify the stacking sequence as [0/90/90/0]. This method can also differentiate between symmetric ($[0/90]_s$, $[90/0]_s$) and non-symmetric cross-ply laminates ($[(0/90)_2]$). Similarly, when inspected from the front and back, the CFRP-4L-2P case results in [0/30] and [90/30] orders or occurrences. This results in the [0/30/30/90]

stacking sequence. The CFRP-4L-3P case results in $[90/45/-45/0]$ from a single-sided inspection since it contains the maximum possible active pairs in a four-layer sample. The CFRP-6L-5P case results in $[-60/90/45/-45/0]$ and $[90/0/-45/45/-60]$ orders of occurrences when inspected from the front and back, respectively. This results in $[-60/90/45/-45/90/0]$ stacking sequence. One important observation from the CFRP-6L-5P case is that, when the laminate was inspected from any of the sides, we could obtain information from the sixth layer. As a result, the proposed method has demonstrated that it is capable of identifying the fiber orientations and stacking sequences up to six layers on one side of the laminate's geometric midplane. Usually, a quasi-isotropic laminate contains an equal number of identical layers at k orientations such that the angles between the layers are $180 * (i/k)$ where $i = 0, 1, ..k-1$ and $k >= 3$ (For example, $[0/\pm 60]_s$, $[0/\pm 45/90]_s$). Based on the samples demonstrated in this study, quasi-isotropic laminates having orientations $k <= 6$, which results in 12 layers, can be completely characterized using the proposed approach. The stacking sequence of the laminates identified using inverse 2D-FFT analysis is given in table 3.

Table 3
Stacking sequence of the laminates identified from inverse 2D-FFT analysis

Sample Label	Design Layup	Order of appearance		Obtained stacking sequence
		Front side inspection	Back side inspection	
CFRP-4L-1P	[0/90/90/0]	[0/90]	[90/0]	[0/90/90/0]
CFRP-4L-2P	[0/30/30/90]	[0/30/90]	[90/30/0]	[0/30/30/90]
CFRP-4L-3P	$[90/\pm 45/0]$	$[90/\pm 45/0]$	$[0/\mp 45/90]$	$[90/\pm 45/0]$
CFRP-6L-5P	$[-60/90/\pm 45/90/0]$	$[-60/90/\pm 45/0]$	$[0/90/\mp 45/-60]$	$[-60/90/\pm 45/90/0]$

4. Summary and Conclusion

In CFRP laminates, a minimum of two layers of unidirectional fabric aligned in different directions (active pair) is required to observe heating due to the induction process. A laminate contains multiple layers that result in multiple active pairs. A circular induction coil was used to ensure that all the available active pairs in the laminate participated in the induction heating process. The CFRP laminates produce distinctive heating patterns governed by the fiber orientations and the degree of electrical contact between various layers. This non-conventional heating behavior has been extensively studied in this paper to identify the fiber orientations and characterize the stacking order within the material. The methodology used for this study is based on the two-dimensional Fast Fourier transformation (2D-FFT) of thermal images, with the heating patterns obtained with thermography. The proposed method has been demonstrated in, but is not limited to, laminates with high junction resistance between adjacent fiber layers. Four different layup configurations were considered in the experiment, $[0/90/90/0]$, $[0/30/30/90]$, $[90/\pm 45/0]$, and $[-60/90/\pm 45/90/0]$ that provides one, two, three and five different active pairs. The key conclusions from this work are:

- The surface heating patterns of CFRP samples obtained through the induction heating process contain pertinent

information on the orientations of the fibers in the laminate. A circular induction coil can excite all the available active pairs of fiber layers in a composite which results in particular spatial surface heating patterns.

- As the number of active pairs increases, identifying fiber orientations from the time domain thermograms becomes difficult. A two-dimensional Fast Fourier transform-based image processing tool is thus proposed here to extract the spatial features of heating patterns and, consequently, the fiber orientations. The proposed approach has been successfully demonstrated to identify fiber orientations.
- The inverse Fourier transform is employed to analyze the occurrence of each layer in the sample. The thermal image sequence was reconstructed using inverse Fourier transformation after applying angle-specific band pass filters. The reconstructed thermal image sequence contains exclusive information on temperature evolution according to the angle specified by the bandpass filters. The temporal shift observed in the reconstructed thermal image sequence provides the order of pattern occurrence in the sample.
- The maximum error obtained in identifying the fiber orientations compared to the design orientations using the proposed approach is 6^o.
- The proposed approach can be implemented on both sides of a quasi-isotropic laminate having orientations $k <= 6$ (12 layers) to identify the fiber orientations and the stacking sequence.

An added advantage that this approach offers is that it can be extended to identify internal defects in CFRP laminates, such as fiber misalignment, fiber breakages, or waviness. We believe that model-assisted reconstruction involving heat diffusion and associated time delays can provide valuable insights into depth estimation as well.

References

[1] V. S. Balakrishnan, H. Seidlitz, Potential repair techniques for automotive composites: A review, Composites Part B: Engineering 145 (2018) 28–38.

[2] C. Soutis, Carbon fiber reinforced plastics in aircraft construction, Materials Science and Engineering: A 412 (2005) 171–176.

[3] N. Hancox, The compression strength of unidirectional carbon fibre reinforced plastic, Journal of Materials Science 10 (1975) 234–242.

[4] T. Yokozeki, T. Ogasawara, T. Ishikawa, Nonlinear behavior and compressive strength of unidirectional and multidirectional carbon fiber composite laminates, Composites Part A: Applied Science and Manufacturing 37 (2006) 2069–2079.

[5] E. Fuoss, P. V. Straznicky, C. Poon, Effects of stacking sequence on the impact resistance in composite laminates—part 1: parametric study, Composite structures 41 (1998) 67–77.

[6] M. Caminero, I. García-Moreno, G. Rodríguez, Damage resistance of carbon fibre reinforced epoxy laminates subjected to low velocity impact: Effects of laminate thickness and ply-stacking sequence, Polymer Testing 63 (2017) 530–541.

[7] L. Cheng, P. Gong, Q. Wang, M. Zou, Y. Zhang, Z. Liu, Effects of ply thickness deviation and ply angle misalignment on the surface accuracy of cfrp laminates, Composite Structures 270 (2021) 114073.

[8] S. Tanaka, T. Ikeda, A. Senba, Sensitivity analysis of thermal deformation of cfrp laminate reflector due to fiber orientation error, Journal of Mechanical Science and Technology 30 (2016) 4423–4426.

[9] V. Kunc, S. W. Case, H. J. Santos-Villalobos, S. Simunovic, The stiffness tensor for composites with curved discontinuous fibers, Composites Part A: Applied Science and Manufacturing 72 (2015) 239–248.

[10] G. Requena, G. Fiedler, B. Seiser, P. Degischer, M. Di Michiel, T. Buslaps, 3d-quantification of the distribution of continuous fibres in unidirectionally reinforced composites, Composites Part A: Applied Science and Manufacturing 40 (2009) 152–163.

[11] A. Bhattacharya, C. Heinzl, A. Amirkhanov, J. Kastner, R. Wenger, Metatracts-a method for robust extraction and visualization of carbon fiber bundles in fiber reinforced composites, in: 2015 IEEE Pacific Visualization Symposium (PacificVis), IEEE, 2015, pp. 191–198.

[12] A. Yoshimura, R. Hosoya, J. Koyanagi, T. Ogasawara, X-ray computed tomography used to measure fiber orientation in cfrp laminates, Advanced Composite Materials 25 (2016) 19–30.

[13] B. R. Denos, D. E. Sommer, A. J. Favaloro, R. B. Pipes, W. B. Avery, Fiber orientation measurement from mesoscale ct scans of prepreg platelet molded composites, Composites Part A: Applied Science and Manufacturing 114 (2018) 241–249.

[14] K. Vanclooster, S. V. Lomov, I. Verpoest, Experimental validation of forming simulations of fabric reinforced polymers using an unsymmetrical mould configuration, Composites Part A: Applied Science and Manufacturing 40 (2009) 530–539.

[15] S. Zambal, W. Palfinger, M. Stöger, C. Eitzinger, Accurate fibre orientation measurement for carbon fibre surfaces, Pattern Recognition 48 (2015) 3324–3332.

[16] M. Schöberl, K. Kasnakli, A. Nowak, Measuring strand orientation in carbon fiber reinforced plastics (cfrp) with polarization, in: World conference on non-destructive testing, 2016, pp. 1–8.

[17] R. Spencer, S. Alwekar, E. Jo, A. A. Hassen, S. Kim, U. Vaidya, Fiber orientation evaluation in reinforced composites using digital image correlation and thermal excitation, Composites Part B: Engineering 234 (2022) 109713.

[18] G. Bardl, A. Nocke, C. Cherif, M. Pooch, M. Schulze, H. Heuer, M. Schiller, R. Kupke, M. Klein, Automated detection of yarn orientation in 3d-draped carbon fiber fabrics and preforms from eddy current data, Composites Part B: Engineering 96 (2016) 312–324.

[19] R. R. Hughes, B. Drinkwater, R. Smith, Characterisation of carbon fibre-reinforced polymer composites through radon-transform analysis of complex eddy-current data, Composites Part B: Engineering 148 (2018) 252–259.

[20] Q. Yi, P. Wilcox, R. Hughes, Modelling and evaluation of carbon fibre composite structures using high-frequency eddy current imaging, Composites Part B: Engineering 248 (2023) 110343.

[21] I.-Y. Yang, K.-H. Im, D. K. Hsu, V. Dayal, D. Barnard, J.-H. Kim, C.-S. Cha, Y.-T. Cho, D.-J. Kim, Feasibility on fiber orientation detection of unidirectional cfrp composite laminates using one-sided pitch–catch ultrasonic technique, Composites science and technology 69 (2009) 2042–2047.

[22] K. Sun-Kyu, H. David, S. Young-Hwan, I. Kwang-Hee, Detection of stacking orientation error of cfrp composite laminates using ultrasound

waves, Transactions of Nonferrous Metals Society of China 19 (2009) s124–s127.

[23] L. Nelson, R. Smith, Fibre direction and stacking sequence measurement in carbon fibre composites using radon transforms of ultrasonic data, Composites Part A: Applied Science and Manufacturing 118 (2019) 1–8.

[24] X. P. Maldague, Nondestructive evaluation of materials by infrared thermography, Springer Science & Business Media, 2012.

[25] N. Puthiyaveettil, S. Krishna, R. Kidangan, S. Unnikrishnakurup, C. Krishnamurthy, M. Zeigler, P. Myrach, K. Balasubramaniam, In-line laser thermography for crack detection at elevated temperature: A numerical modeling study, in: 13th International Conference on Quantitative Infrared Thermography, 2016, pp. 4–8.

[26] S. Hedayatrasa, J. Segers, G. Poelman, W. V. Paepegem, M. Kersemans, Vibro-thermal wave radar: Application of barker coded amplitude modulation for enhanced low-power vibrothermographic inspection of composites, Materials 14 (2021) 2436.

[27] R. T. Kidangan, C. V. Krishnamurthy, K. Balasubramaniam, Identification of the fiber breakage orientation in carbon fiber reinforced polymer composites using induction thermography, NDT & E International 122 (2021) 102498.

[28] K. R. Thomas, K. Balasubramaniam, Scanning induction thermography (sit) for imaging damages in carbon-fibre reinforced plastics (cfrp) components, in: AIP Conference Proceedings, volume 1650, American Institute of Physics, 2015, pp. 306–313.

[29] R. T. Kidangan, C. V. Krishnamurthy, K. Balasubramaniam, Detection of dis-bond between honeycomb and composite facesheet of an inner fixed structure bond panel of a jet engine nacelle using infrared thermographic techniques, Quantitative InfraRed Thermography Journal 19 (2022) 12–26.

[30] P. Myrach, B. Polomski, E. Le Claire, S. Unnikrishnakurup, N. Vengara, K. Balasubramaniam, M. Ziegler, Thermographic crack detection in hot steel surfaces, in: 19th World Conference on Non-Destructive Testing 2016, Munich, Germany, 2016, pp. 1–8.

[31] S. Unnikrishnakurup, J. Dash, S. Ray, B. Pesala, K. Balasubramaniam, Nondestructive evaluation of thermal barrier coating thickness degradation using pulsed IR thermography and THz-TDS measurements: A comparative study, NDT and E International 116 (2020). doi:10.1016/j.ndteint.2020.102367.

[32] H. Fernandes, H. Zhang, C. Ibarra-Castanedo, X. Maldague, Fiber orientation assessment on randomly-oriented strand composites by means of infrared thermography, Composites Science and Technology 121 (2015) 25–33.

[33] F. Wang, J. Liu, Y. Liu, Y. Wang, Research on the fiber lay-up orientation detection of unidirectional cfrp laminates composite using thermal-wave radar imaging, Ndt & E International 84 (2016) 54–66.

[34] H. Fernandes, H. Zhang, A. Figueiredo, F. Malheiros, L. H. Ignacio, S. Sfarra, C. Ibarra-Castanedo, G. Guimaraes, X. Maldague, Machine learning and infrared thermography for fiber orientation assessment on randomly-oriented strands parts, Sensors 18 (2018) 288.

[35] G. Wasselynck, D. Trichet, B. Ramdane, J. Fouldagar, Interaction between electromagnetic field and cfrp materials: a new multiscale homogenization approach, IEEE Transactions on Magnetics 46 (2010) 3277–3280.

[36] B. K. Fink, R. L. McCullough, J. W. Gillespie Jr, A local theory of heating in cross-ply carbon fiber thermoplastic composites by magnetic induction, Polymer Engineering & Science 32 (1992) 357–369.

[37] A. Miller, The nature of induction heating in graphite-fiber, polymer-matrix composite materials, Sampe Journal 26 (1990) 37–54.

[38] R. Prakash, C. Owston, Eddy-current method for the determination of lay-up order in cross-plied crfp laminates, Composites 7 (1976) 88–92.

[39] A. K. Miller, W. Lin, Joining of composite materials by induction heating, 1993. US Patent 5,240,542.

[40] W. Lin, Induction heating model for graphite fiber/thermoplastic matrix composites, Sampe Journal 27 (1991) 45–51.

[41] W. Lin, A. K. Miller, O. Buneman, Predictive capabilities of an induction heating model for complex-shape graphite fiber/polymer matrix composites, in: 24th International SAMPE Technical Conference, volume 24, 1992, pp. T606–T620.

[42] B. K. Fink, R. L. McCullough, J. W. Gillespie Jr, A model to predict the planar electrical potential distribution in cross-ply carbon-fiber composites subjected to alternating magnetic fields, Composites science and technology 49 (1993) 71–80.

[43] B. K. Fink, R. L. McCullough, J. W. Gillespie Jr, A model to predict the through-thickness distribution of heat generation in cross-ply carbon-fiber composites subjected to alternating magnetic fields, Composites science and technology 55 (1995) 119–130.

[44] B. K. Fink, R. L. McCullough, J. W. Gillespie Jr, Experimental verification of models for induction heating of continuous-carbon-fiber composites, Polymer Composites 17 (1996) 198–209.

[45] S. Yarlagadda, H. J. Kim, J. W. Gillespie Jr, N. B. Shevchenko, B. K. Fink, A study on the induction heating of conductive fiber reinforced composites, Journal of composite materials 36 (2002) 401–421.

[46] S. Yarlagadda, Heating mechanisms in induction processing of carbon fiber reinforced thermoplastic prepreg, in: 45th International SAMPE Symposium and Exhibition, 2000, pp. 79–89.

[47] H. Kim, S. Yarlagadda, J. W. Gillespie, N. B. Shevchenko, B. K. Fink, A study on the induction heating of carbon fiber reinforced thermoplastic composites, Advanced Composite Materials 11 (2002) 71–80.

[48] H. J. Kim, S. Yarlagadda, N. B. Shevchenko, B. K. Fink, J. W. Gillespie Jr, Development of a numerical model to predict in-plane heat generation patterns during induction processing of carbon fiber-reinforced prepreg stacks, Journal of composite materials 37 (2003) 1461–1483.

[49] F. Lundström, K. Frogner, M. Andersson, A numerical model to analyse the temperature distribution in cross-ply cfrp during induction heating, Composites Part B: Engineering 202 (2020) 108419.

[50] R. T. Kidangan, S. Unnikrishnakurup, C. V. Krishnamurthy, K. Balasubramaniam, The influence of interlaminar microstructure on the induction heating patterns of cfrp laminates, Materials Today Communications 33 (2022) 104338.

[51] E. J. Wood, Applying fourier and associated transforms to pattern characterization in textiles, Textile Research Journal 60 (1990) 212–220.

[52] S. A. Hosseini Ravandi, K. Toriumi, Fourier transform analysis of plain weave fabric appearance, Textile Research Journal 65 (1995) 676–683.

[53] D.-M. Tsai, C.-Y. Hsieh, Automated surface inspection for directional textures, Image and Vision computing 18 (1999) 49–62.

[54] A. Sakaguchi, G. H. Wen, Y.-I. Matsumoto, K. Toriumi, H. Kim, Image analysis of woven fabric surface irregularity, Textile Research Journal 71 (2001) 666–671.

[55] MATLAB, MathWorkscom, https://uk.mathworks.com/help/matlab/ref/fft2.html, 2022. Accessed: 2023-02-23.

[56] J. W. Goodman, Introduction to Fourier optics, Roberts and Company publishers, 2005.